Regenerative Therapy 26 (2024) 760–766

Contents lists available at ScienceDirect

Regenerative Therapy

journal homepage: http://www.elsevier.com/locate/reth

Original Article

Superior bone regenerative properties of carbonate apatite with locational bone-active factors through an inorganic process

Yuki Sugiura [a, b, *], Fumiko Ono [c], Masakatsu Nohara [c], Mai Funabiki [c], Kenji Kutara [c], Teppei Kanda [c], Etsuko Yamada [a], Masanori Horie [a]

[a] Health and Medical Research Institute, National Institute of Advanced Industrial Science and Technology (AIST), 2217-14, Hayashi-cho, Takamatsu, Kagawa, 761-0395, Japan
[b] Health and Medical Research Institute, National Institute of Advanced Industrial Science and Technology (AIST), 1-1-1, Higashi, Tsukuba, Ibaragi, 305-3095, Japan
[c] Department of Veterinary Associated Science, Faculty of Veterinary Medicine, Okayama University of Science (OUS), 1–3 Ikoi-no-oka, Imabari, Ehime, 794-8555, Japan

ARTICLE INFO

Article history:
Received 19 August 2024
Accepted 29 August 2024

Keywords:
Periodontic
Bioceramics
Bone regeneration
Silica
Carbonate apatite

ABSTRACT

Rapid bone regeneration is crucial for restoring alveolar bone and oral functions following periodontal diseases. However, the development of effective biomedical materials for this purpose remains insufficient. While bone autografts can enhance bone regeneration, they are invasive to healthy areas. Specifically, for alveolar bone regeneration, the implanted material must possess adequate mechanical strength. Moreover, local administration is preferred for older adults, who are a primary target population, to maintain their quality of life. We developed a silica-substituted carbonate apatite (CO_3Ap−silica) block as newly bone substitute with a bone growth factor, featuring the major inorganic component of mature bone to enhance bone regeneration. CO_3Ap−silica block stimulated the bone remodeling process at the implantation site and demonstrated significantly better bone regeneration compared to currently used carbonate apatite substitutes. Therefore, this new material is expected to advance technologies for restoring occlusal function after periodontal disease.

1. Introduction

For dental periodontal diseases, rapid bone regeneration is a crucial technology for recovery in the global elderly population [1,2]. Historically, bone autografts have been regarded as the gold standard for treating bone defects. However, limitations such as the limited amount of harvestable bone, the invasiveness of the procedure, and the increased risk of infection present significant challenges [3–5]. The clinical field demands bone regeneration substitutes produced through chemical processes that offer unlimited availability and eliminate infection risks, unlike autografts or allografts with unknown etiological risks.

In response to this demand, bioceramic-based bone substitutes have been introduced [6]. Carbonate apatite [CO_3Ap: $Ca_{10-a}(PO_4)_6(CO_3)_c(OH)_{2-d}$], the primary inorganic component of aged bone mineral, has been proposed as a bone substitute [7–9]. CO_3Ap bone substitutes are expected to exhibit high osteoconductivity and effectively reconstruct and regenerate defects [10]. However, bone regeneration using these materials remains slow, prolonging the recovery of skeletal functions [11]. For older patients, prolonged rest can deteriorate their overall condition [12,13]. Therefore, rapid regeneration of the treated area is essential.

Silica shows promise as a support material to promote skeletal growth when administered [14–16]. However, organic materials such as tetraethyl orthosilicate, used for silica loading, have risks owing to residual organic molecules [17–19].

Our previous work introduced a wet synthesis method for silica-supported calcium phosphate [20–23]. We discovered that the mechanical strength of octacalcium phosphate [OCP: $Ca_8(PO_4)_4(HPO_4)_2 \cdot 5H_2O$] improves when loaded with silica and dicarboxylic acid molecules simultaneously [24]. In this process,

* Corresponding author. Health and Medical Research Institute, National Institute of Advanced Industrial Science and Technology (AIST), 2217-14, Hayashi-cho, Takamatsu, Kagawa, 761-0395, Japan.
E-mail address: yuki-sugiura@aist.go.jp (Y. Sugiura).
Peer review under responsibility of the Japanese Society for Regenerative Medicine.

https://doi.org/10.1016/j.reth.2024.08.021

dicarboxylic acid molecules leach out during the phase transition to apatite, while silica remains in the interlayer [20,25]. Thus, OCP loaded with both silica and dicarboxylic acid molecules can transition to silica-substituted apatite with enhanced strength. In this study, we aimed to prepare silica-loaded apatite via phase transition from OCP and evaluate its bone regeneration ability.

2. Result and discussion

As an initial trial in this study, we investigated the preparation of silica-substituted apatite blocks with sufficient mechanical strength from both dicarboxylic acid (succinate) and silica-substituted OCP blocks through a hydrolysis reaction. Preprepared succinate–silica composite-supported OCP blocks were immersed in $(NH_4)_2CO_3$ solution. The immersed samples maintained the shape of the OCP blocks (Fig. 1a). After immersion, XRD patterns indicated the disappearance of the OCP peak and the appearance of the apatite peak (Fig. 1b). In samples treated with $(NH_4)_2CO_3$ solutions concentrations above 2 mol/L, a calcite peak was also observed. Fourier transform infrared (FT–IR) spectra showed several bands around 1420 and 1460 cm^{-1}, indicating B-type CO_3Ap carbonate adsorption (Fig. 1c). The intensities of these bands increased with higher $(NH_4)_2CO_3$ concentrations [26,27]. Notably, no dicarboxylic acid bands were observed after immersion. Additionally, silanol bands were clearly present, indicating that silica remained substituted in the apatite blocks. CHN analysis supported the FT–IR results, showing a monotonic increase in CO_3 content with increasing $(NH_4)_2CO_3$ concentration (Fig. 1d). The silica content slightly decreased with higher $(NH_4)_2CO_3$ concentrations (Fig. 1e). The pH of the solutions after impregnation decreased slightly in both cases (Fig. 1f).

Having prepared the silica-substituted apatite in bulk, we proceeded to evaluate its mechanical strength, which is crucial for its use as a bone regeneration material, requiring at least 0.2 MPa. Impregnation in solution initially reduced the mechanical strength (Fig. 2a). However, the mechanical strength of the blocks increased with higher $(NH_4)_2CO_3$ concentrations (Fig. 2b) [28,29]. The system with the highest carbonate content and single-phase apatite, treated with 1.0 mol/L $(NH_4)_2CO_3$, showed a DTS strength of approximately 0.7 MPa. This strength was significantly higher than that of the initially prepared CO_3Ap–silica from only silica-substituted OCP (<0.1 MPa) and was sufficient for implantation in animals. The stress–strain curves exhibited similar behavior. Fig. 2c shows SEM micrographs of the samples. The cross-sectional microstructure of the specimens was examined to understand the reason for their high mechanical strength. A structure of closely packed, plate-like crystals was observed regardless of the carbonate content. This suggests that the samples exhibited high mechanical strength because they were not scabbed. Additionally, the density was significantly higher than that of the initially prepared silica-loaded CO_3Ap.

We obtained silica-loaded carbonate apatite with sufficient strength and evaluated its bone regenerative capacity *in vivo*. As a reference, CO_3Ap blocks without silica were used, which are analogous to a commercially available bone regeneration material [6]. The prepared blocks were implanted into rabbit femur defects (Fig. 3a). One month after implantation, bone tissue formed firmly around both samples, demonstrating high osteoconductivity (Fig. 3b). However, the new bone surrounding the CO_3Ap–silica material was notably thicker. Significant resorption of CO_3Ap–silica was observed three months after implantation, along with partial bone regeneration at the implantation site. In all cases, a clear bond was evident between the bone tissue and the specimen (Fig. 3c). The ratio of new bone formed at the implantation site tended to be higher for CO_3Ap-silica than for CO_3Ap. The percentage of new bone formation at the implantation site tended to be higher for CO_3Ap-silica than for CO_3Ap at the 3 month follow-up (Fig. 3d). The ratio of the remaining specimen and bone contact were as follows

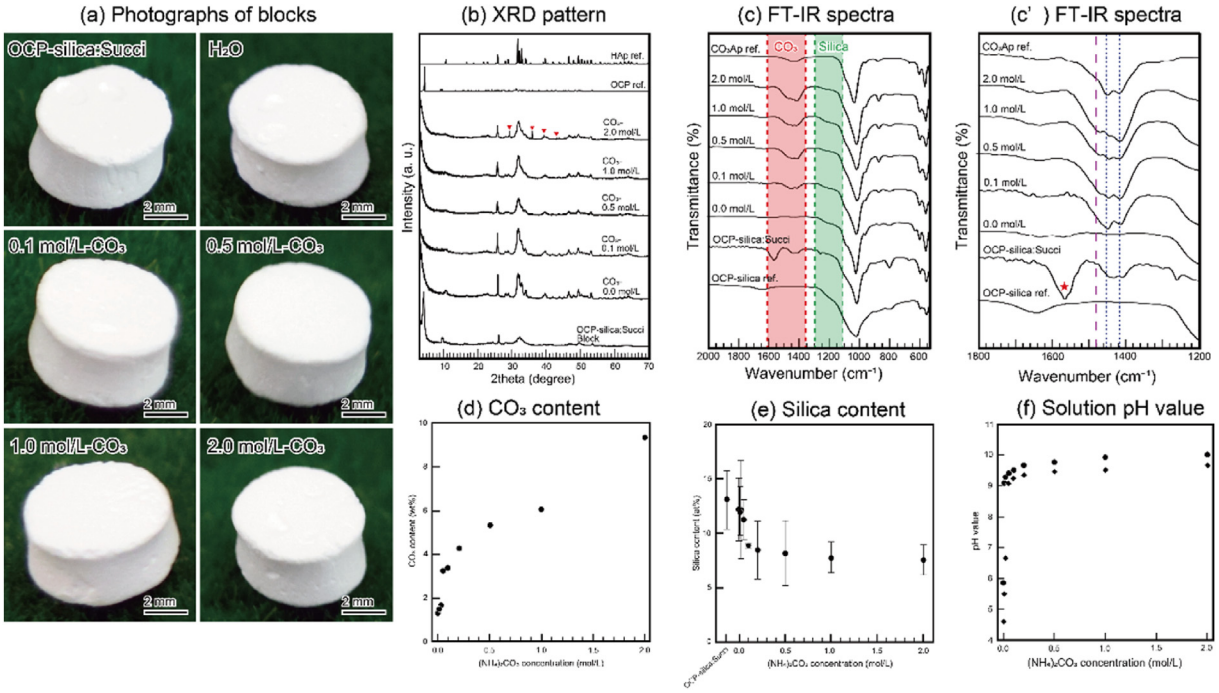

Fig. 1. Material characterization of apatite-silica blocks with different CO_3 amounts from OCP-silica:Succinate blocks. (a) Photographs of the blocks before and after $(NH_4)_2CO_3$ solution immersion. (b) Bulk XRD patterns of the blocks before and after $(NH_4)_2CO_3$ solution immersion. (c) FT-IR spectra of the blocks before and after $(NH_4)_2CO_3$ solution immersion. (c') Expanded around 1200-1800 cm^{-1} of (c). (d) CO_3 contents of the blocks after $(NH_4)_2CO_3$ solution immersion. (e) Si contents of the blocks after $(NH_4)_2CO_3$ solution immersion. (f) The pH values of $(NH_4)_2CO_3$ solutions before (●) and after immersion (◆).

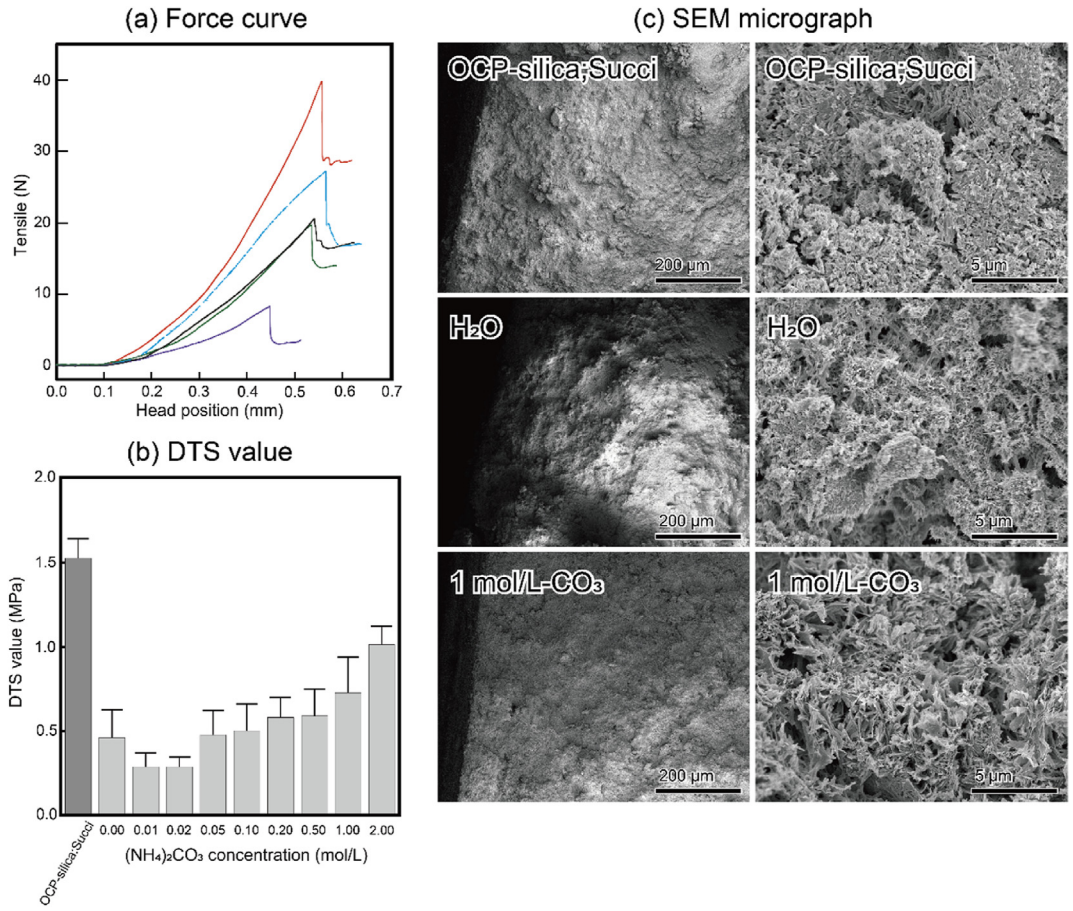

Fig. 2. Mechanical properties and fine structures of apatite-silica blocks with different CO_3 amounts from OCP-silica:Succinate blocks. (a) Typical force curves of the samples. Red: OCP-silica:Succinate block. Purple: H_2O immersion. Green: 0.1 mol/L $(NH_4)_2CO_3$ immersion. Black: 0.5 mol/L $(NH_4)_2CO_3$ immersion. Blue: 1.0 mol/L (NH4)2CO3 immersion. (b) DTS values of the OCP-silica:Succinate blocks before and after immersion. (c) SEM micrographs of cross sections of the OCP-silica:Succinate blocks and after immersion into H_2O and 1.0 mol/L $(NH_4)_2CO_3$.

(Fig. 3e). Both the bone contact rate and bone replacement rate were significantly higher for CO_3Ap–silica compared to CO_3Ap (Fig. 3f). The bone in contact with CO_3Ap–silica was more substantial than that with carbonate apatite. Additionally, bone marrow tissue surrounding the bone, rich in reticulocytes and low in fatty structure, was observed (Fig. 3g).

This material's high bone contact rate and bone replacement properties were evaluated in greater detail to confirm its impact on the bone remodeling process. Tartaric acid-resistant acid phosphatase (TRAP) staining, which highlights osteoclasts, was used to assess bone remodeling activity (Fig. 4a). CO_3Ap–silica exhibited a significantly higher density of osteoclasts at both implantation periods (Fig. 4b), despite silica's known inhibitory effect on osteoclast differentiation [16,30]. Both osteoblast and osteoclast density tended to be significantly higher in CO_3Ap-silica than in CO_3Ap. Osteoblast density was observed to decrease over time in both samples. This was also consistent with the rate of new bone formation (Fig. 4c and d). This relationship between osteoclast activity and new bone formation suggests that in silica-loaded carbonate apatite, osteoblast activity and bone remodeling are more active, leading to enhanced bone regeneration at the implantation site.

CO_3Ap–silica has demonstrated promising results as a bone regeneration material. One of its advantages over silica-loaded OCP is its high osteoconductivity from the early implantation stage, which may prevent strength loss at the bone implantation site. The higher bone conductivity of CO_3Ap compared to OCP can be attributed to differences in their solubility [31,32]. Specifically, the higher acid resistance of CO_3Ap to osteoclast-produced acid may harmonize the bone remodeling process with the material's regenerative capacity.

CO_3Ap–silica is expected to continuously supply silica in the immediate vicinity in response to osteoclastic activity. The dissolved silica reduces osteoclastic activity while significantly enhancing osteoblastic activity [33]. This increased osteoblast activity likely drives bone regeneration and an active bone remodeling process primarily mediated by osteoblasts.

Historically, bone replacement materials have been designed to promote bone regeneration in harmony with the bone remodeling process [6,34]. However, in elderly patients whose bone remodeling processes have declined, current bone replacement materials exhibit low regenerative capacity [34]. Additionally, autologous bone grafting is often not an option. Bone loss is typically a local issue. Thus, it is desirable to induce rapid bone regeneration, specifically in the defect area. Moreover, there is a need for processes that enhance bone remodeling, the metabolic aspect of bone health, rather than drugs that inhibit bone metabolism, such as bisphosphonates [35–37]. CO_3Ap–silica, with its sufficient mechanical strength, biocompatibility of carbonate apatite, and ability to activate osteoblasts and the bone remodeling process, shows great potential. Evidence of this includes the formation of red marrow-like tissue with high bone regeneration capacity around CO_3Ap–silica. In this study, we evaluated CO_3Ap–silica in the form of a dense block, which is suitable for such assessments. Future

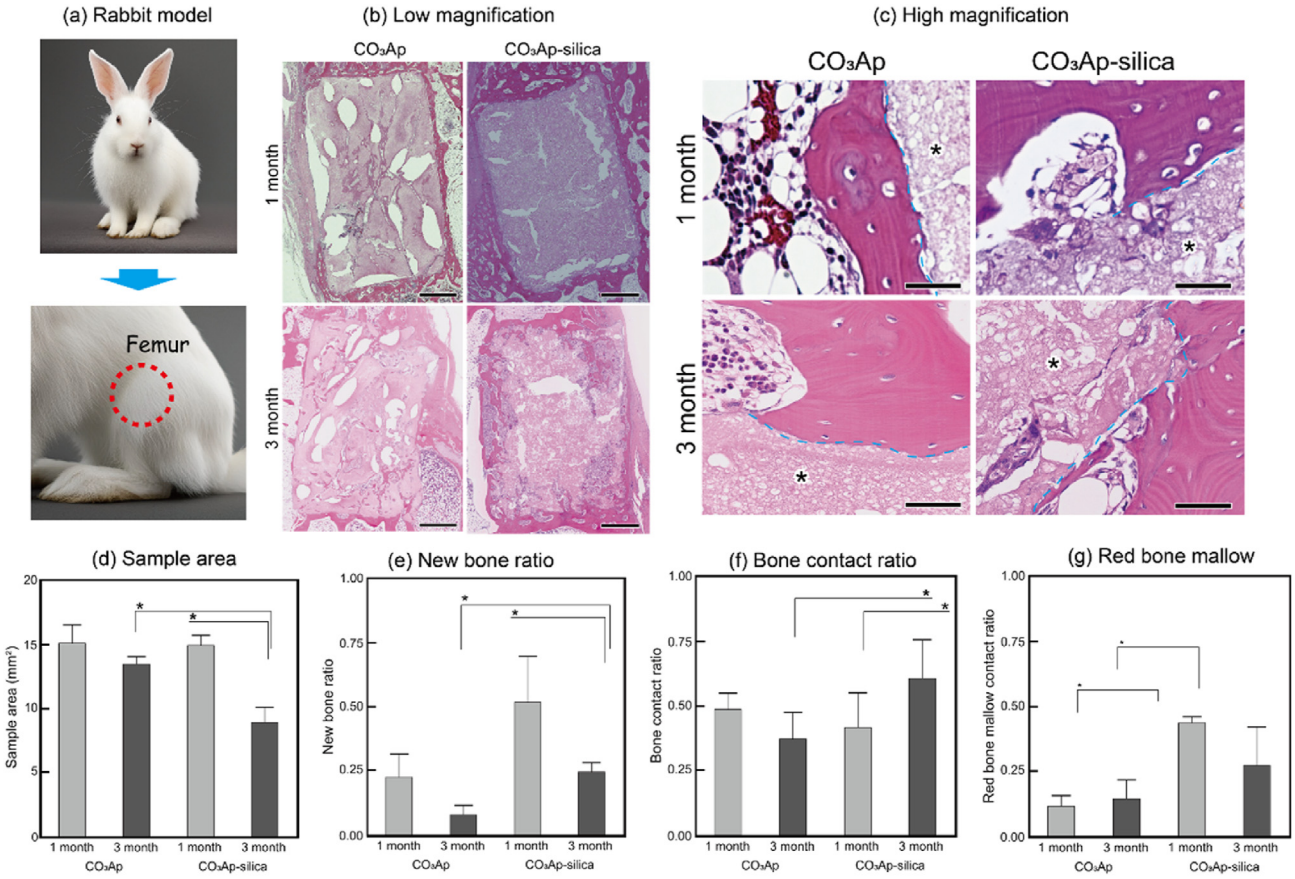

Fig. 3. *In vivo* evaluation results of feasibility studies for CO_3Ap-silica bone regeneration ability using rabbit femur bone defect model. (a) Schematic illustration of implanted site. (b) Histological images of CO_3Ap (reference) and CO_3Ap-silica blocks 1 and 3 months after implantation. (c) Magnified images of the boundary of samples and tissues 1 and 3 months after implantation. *: samples. Blue broken lines: the boundary of samples and bone tissues. (d) Statical analysis results of sample area. (e) Statical analysis results of newly bone formed ratio. (f) Statical analysis results of bone contact onto samples. (g) Statical analysis results of red bone mallow contact onto samples. *: $p < 0.05$.

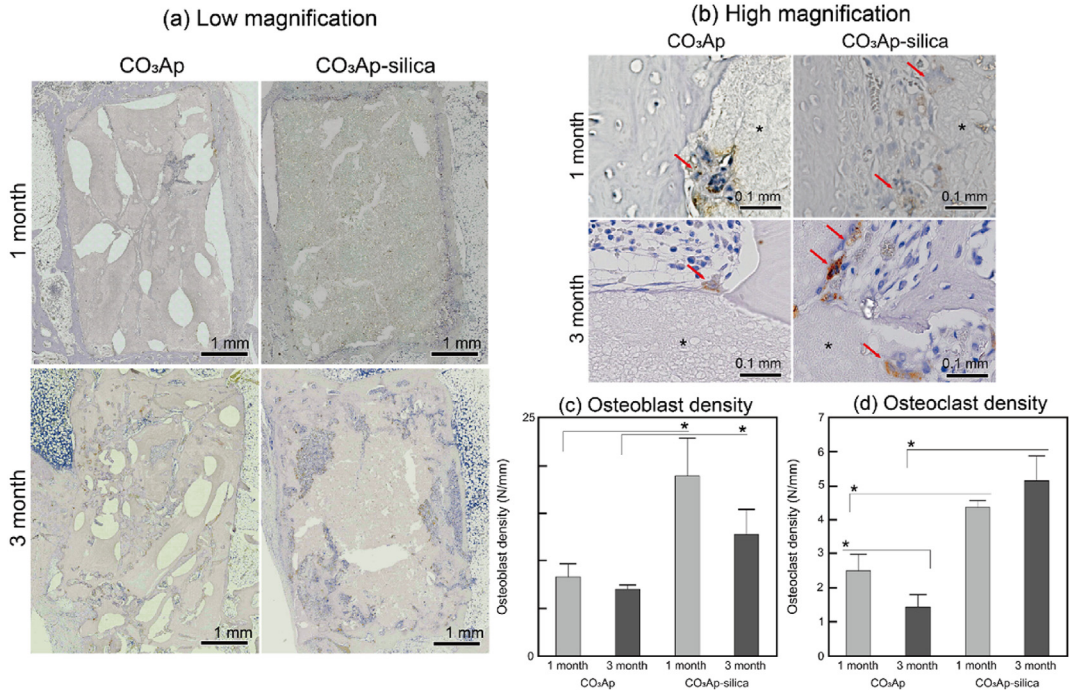

Fig. 4. TRAP-stained histological images of CO_3Ap and CO_3Ap-silica blocks 1 and 3 months after implantation. (a) Low magnified images of CO_3Ap (reference) and CO_3Ap-silica blocks 1 and 3 months after implantation. (b) Magnified TRAP stained histological images of CO_3Ap and CO_3Ap-silica blocks 1 and 3 months after implantation. *: materials. Red arrow: TRAP-positive multinuclear giant cells. (c) Statical analysis result of the density of osteoblast. (d) Statical analysis result of the density of osteoclast. *: $p < 0.05$.

developments are expected to demonstrate even higher bone regenerative capacity by incorporating mechanical structures, such as foam and cementing processes, which further induce bone formation [38–40].

Currently, the primary cause of tooth loss is not dental caries but the dissolution and loss of the alveolar bone that supports the teeth owing to periodontal disease [41–43]. The resulting loss of occlusal function and deterioration of the oral environment can contribute to the expansion of oral flora and lead to serious conditions such as aspiration pneumonia and cardiac disease [44,45]. Reconstruction and regeneration of the alveolar bone are essential to restore occlusal function. Although treatments involving heat-generating nanoparticles, fungal breakdown factor particles, and growth factors have been proposed for periodontal disease, they do not address cases where the alveolar bone itself has been lost [46–49]. This material can serve as a base for nanoparticles and tissue growth factors, potentially enabling early recovery of bone volume and formation. Combining it with these materials may prevent tooth loss and maintain occlusal function in patients with periodontal disease.

3. Conclusion

In this study, we fabricated silica-containing CO_3Ap blocks with sufficient strength (DTS: ~1 MPa) and evaluated their bone regeneration potential using a rabbit femur defect model to assess their usefulness for CO_3Ap. This silica substitution enhanced periosteal bone production. Despite the silica substitution, CO_3Ap's high biocompatibility and osteoconductivity remained unchanged. The development of this new material will address the non-adaptability of bone replacement materials, particularly for older adults, owing to the low bone regeneration capacity of current materials.

4. Materials and methods

4.1. Fabrication of silica-substituted apatite blocks with different CO_3 contents

All reagents were purchased from FUJI Film Wako Pure Inc., Japan. We prepared stock solutions of 4.0 mol/L H_3PO_4 and 2.0 mol/L $(NH_4)_2CO_3$ by diluting and dissolving them in distilled water.

As an initial step, we fabricated OCP blocks containing succinate and silica (OCP–silica) as intermediate materials. The details of the OCP–silica blocks are described in a published study [24]. Briefly, the fabrication process of the OCP component is as follows. First, 2.0 mL of H_3PO_4 and 0.60 g of succinate were placed into an agate mortar and dissolved. Then, 1.2 g of $CaCO_3$ powder was gradually mixed into the solution. Subsequently, 1.08 mL of 38 wt% Na_2SiO_3 was added while stirring with a pestle. To promote the interlocking of the formed OCP–silica crystals, the mixture was placed in a silicone rubber mold ($\varphi 6 \times 3$ mm) and tightly sealed with a 0.3 mm thick polypropylene sheet to prevent evaporation. The reaction process was performed at 60 °C for 1 day. Finally, the treated materials were thoroughly washed with distilled water three times and then dried in a 40 °C oven for 1 day.

After fabricating and evaluating the OCP–silica blocks, 10 pieces of these blocks were immersed in 20 mL of 0.0–2.0 mol/L $(NH_4)_2CO_3$ at 80 °C for 5 days. The treated blocks were washed with distilled water thrice and then dried in an 80 °C oven for 1 day. The pH of the solutions before and after immersion was measured using a pH electrode (ThoupH 9615S-10D, Horiba Co., Kyoto, Japan) connected to a multimeter (LAQUA F–2000PC, Horiba Co., Kyoto, Japan).

4.2. Fabricated material characterization and evaluation

Crystallographic information about the samples was obtained via X-ray diffraction (XRD: MiniFlex600, Rigaku Co., Japan) at an acceleration voltage of 40 kV and a current of 15 mA. All samples were finely crushed using an agate mortar and pestle, and the resulting powder was mounted onto a φ10 mm $\times$ 0.2 mm Si non-reflective plate. The diffraction angle was continuously scanned over 2θ values ranging from 3° to 70° at a scanning rate of 5°/min for characterization and from 2° to 12° and 20°–40° at a scanning rate of 1°/min for crystallographic parameter analysis.

The chemical bonding structure of the samples was analyzed via Fourier transform infrared spectroscopy (FT–IR: IRTracer-100, Shimadzu Co., Japan) using a triglycine sulfate detector (30 scans, resolution 2 cm^{-1}) with a diamond attenuated total reflection prism. The atmospheric background was used for the measurements.

The fine structure of the samples was examined using field emission scanning electron microscopy (FE–SEM: JSM-6700F, JEOL Co., Japan) at an acceleration voltage of 3 kV after Os sputtering.

The Ca and P (PO_4) (and Na) contents of the samples were measured by inductively coupled plasma atomic emission spectroscopy (ICP–AES: 5110VDV, Agilent Technology Co., Japan) after the samples were completely dissolved in a 2 wt% HNO_3 solution.

The Si content of the samples was measured by energy-dispersive X-ray fluorescence spectroscopy (EDX-8100, Shimadzu Co., Japan) at an acceleration voltage of 15 kV under vacuum conditions. The Si/Ca ratio was determined using disk-shaped sintered blocks with serial mixture ratios of hydroxyapatite and SiO_2.

The carbonate content in each sample was estimated from the at % of C in the CO_3Ap-silica block, as measured with a carbon–hydrogen–nitrogen (CHN) coder (MT-6; Yanako Analytical Instruments, Kyoto, Japan) under O_2 and Ar gas carrier.

The mechanical strengths of cylindrical-shaped specimens were evaluated in terms of the diametral tensile strength (DTS). The diameter and thickness of each specimen were measured using a micrometer (MDC-25MU, Mitutoyo Co. Ltd., Kawasaki, Japan). The specimens were then tested under compression by crushing at a constant crosshead speed of 1 mm/min using a universal testing machine (AGS-J, Shimadzu, Kyoto, Japan). For each specimen, the mean DTS values of five specimens were estimated and reported as the mean ± standard deviation using Student's *t*-test analysis ($p < 0.05$) because all factors were independent.

4.3. In vivo evaluation for bone regeneration properties

All animal experiments were conducted with the approval of the ethics committee of animal experimentation of AIST (approval numbers: A2018–327, A2020–376) and Okayama University of Science (approval number: E2020–096).

Eight male Japanese white rabbits (19 weeks old, each weighing 3.0–3.5 kg) were used in this study. The femurs of both legs of the rabbits, under systemic anesthesia, were carefully exposed by exfoliation. After the dissection of the periosteum, bone defects with dimensions of $\varphi 6.0 \times 3.0$ mm^3 were artificially created in the cancellous bones of both femurs using a trephine bur attached to a dental handpiece. For comparison, the artificial bone defects were reconstructed to the level of the bone surface using CO_3Ap–silica and reference CO_3Ap blocks ($\varphi 6.0 \times 3.0$ mm). The fabrication method for CO_3Ap blocks is detailed in a published study [28].

The specimens were sterilized at 80 °C for 8 h before implantation. Finally, the skin flaps were closed using suture thread. Buprenorphine hydrochloride (LepetanVR, Otsuka Pharmaceutical Co., Japan) and gentamicin sulfate (GENTACINVR, MSD, Tokyo, Japan) were injected intramuscularly to prevent postoperative pain and bacterial infection, respectively.

Four rabbits were euthanized at 1-month post-implantation and the remaining four at 3-months post-implantation by KCl overdose injection. The extracted femurs were fixed in PO_4-buffered 10 % formaldehyde for 7 days. The fixed tissues were then decalcified using ethylenediaminetetraacetic acid (EDTA) or K-CX solution, dehydrated with graded ethanol solutions, and embedded in paraffin. The embedded tissues were sliced into 5–10-μm-thick sections using a microtome. HE and tartrate-resistant acid phosphatase (TRAP) stains were applied to the specimens. An all-in-one microscope (BZ-X710, KEYENCE, Osaka, Japan) was used to observe the stained specimens. The ratios of new bone formation in each sample were measured using ImageJ software (NIH, USA). The total length and area of the samples and tissues were measured using HE-stained histological samples. The results for each sample were statistically analyzed ($\mathbf{N = 4}$).

Statistical analysis was performed using the Student's *t*-test method. A *p*-value of less than 0.05 was considered statistically significant.

4.4. Calculation for tissue response of samples

The data measured using ImageJ software, NIH, USA, were used for the analysis ($\mathbf{N} = 4$ for each sample).

The areas of new bone and reminded samples were calculated as follows. The embedding site of the sample is a 6 × 3 mm rectangle. Then, the surrounded area of the sample including sample (8 × 4 mm rectangle) defined as area of interest; S. The area of newly formed bone; A_b and reminded sample area; A_s were measured. The ratio of newly formed bone; R_b was calculated as:

$$R_b = A_b / (S - A_s) \quad (1)$$

The area of bone tissue and the area of the sample in this area were each measured, and the quotient of the areas was calculated for each sample.

The density of osteoclasts was calculated as follows. The circumferential length of the samples was measured beforehand. The number of TRAP-positive, multinucleated giant cells in contact with the embedded sample was then measured and divided by the circumferential length of the sample to obtain the density of osteoclasts. The density of osteoblasts was determined by measuring the number of osteoblasts distributed either directly above the sample or on bone beams in direct contact with the sample. As in the case of osteoclasts, the density was determined by dividing the number of osteoblasts by the circumferential length of the sample.

Declaration of competing interest

Authors declare no financial interest and no conflict of interest.

Acknowledgement

We thank Dr. T. Nakanishi, RIST, Kagawa, Japan, for performing the FT-IR measurements. This study was financially supported by the AMED Seeds H program (Keio University; grant number H424TS), AMED Seeds A program (Keio University; grant number A424TR), Kazuchika Okura Memorial Foundation 2022FY Grant-in-Aid, and JST-CREST (grant number: JPMJCR22L5).

References

[1] WHO's annual world health statistics reports 2024. Switzerland: World Health Organization; 2024. WHO Press.
[2] Ikemoto T, Arai YC. Locomotive syndrome: clinical perspectives. Clin Interv Aging 2018;13:819–27.
[3] Zhang M, Matinlinna JP, Tsoi JKH, Liu W, Cui X, Lu WW, et al. Recent developments in biomaterials for long-bone segmental defect reconstruction: a narrative overview. J Orthop Translat 2020;22:26–33.
[4] García-Gareta E, Coathup MJ, Blunn GW. Osteoinduction of bone grafting materials for bone repair and regeneration. Bone 2015;81:112–21.
[5] Sutherland AG, Raafat A, Yates P, Hutchison JD. Infection associated with the use of allograft bone from the north east scotland bone bank. J Hosp Infect 1997;35:215–22.
[6] Dorozhkin SV. Bioceramics of calcium orthophosphates. Biomater 2010;31:1465–85.
[7] LeGeros RZ. Calcium phosphate-based osteoinductive materials. Chem Rev 2008;108:4742–53.
[8] Thang LH, Bang LT, Son NA, Ramesh S. Effect of carbonate contents on the thermal stability and mechanical properties of carbonated apatite artificial bone substitute. JMEPEG 2023;32:1006–16.
[9] Deguchi K, Nomura S, Tsuchiya A, Takahashi I, Ishikawa K. Effects of the carbonate content in carbonate apatite on bone replacement. J Tissue Eng Regen Med 2022;16:200–6.
[10] Ishikawa K. Carbonate apatite bone replacement: learn from the bone. J Ceram Soc Jpn 2019;127:595–601.
[11] Kanazawa M, Tsuru K, Fukuda N, Sakemi Y, Nakashima Y, Ishikawa K. Evaluation of carbonate apatite blocks fabricated from dicalcium phosphate dihydrate blocks for reconstruction of rabbit femoral and tibial defects. J Mater Sci Mater Med 2017;28:85–95.
[12] Lammes E, Rydwik E, Akner G. Effects of nutritional intervention and physical training on energy intake, resting metabolic rate and body composition in frail elderly. A randomised, controlled pilot study. J Nutr Health Aging 2012;16:162–7.
[13] Wadsworth D, Lark S. Effects of whole-body vibration training on the physical function of the frail elderly: an open, randomized controlled trial. Arch Phys Med Rehabil 2020;101:1111–9.
[14] Carlisle EM. Silicon: an essential element for the chick. Science 1972;178:619–21.
[15] Xynos ID, Edgar AJ, Buttery LDK, Hench LL, Polak JM. Ionic products of bioactive glass dissolution increase proliferation of human osteoblasts and induce insulin-like growth factor II mRNA expression and protein synthesis. Biochem Biophys Res Commun 2000;276:461–5.
[16] Beck Jr, GR, Ha S-W, Camalier CE, Yamaguchi M, Li Y, Lee J-K, et al. Bioactive silica-based nanoparticles stimulate bone-forming osteoblasts, suppress bone-resorbing osteoclasts, and enhance bone mineral density *in vivo*. Nanomed Nanotechnol Biol Med 2012;8:793–803.
[17] Nakamura J, Kasuga T. Enhancement of crystalline plane orientation in silsesquioxane-containing vaterite particles towards tuning of calcium ion release. J Mater Chem B 2014;2:1250–4.
[18] Obata A, Mori K, Inukai K, Kato K, Poologasundarampillai G, Kasuga T. Three-Dimensional cotton-wool-like polyhydroxybutyrate/siloxane-doped vaterite composite fibrous scaffolds: effect of imogolite-coating on physicochemical and cell adhesion properties. Front Mater 2020;7:33.
[19] Obata A, Tokuda S, Kasuga T. Enhanced in vitro cell activity on silicon-doped vaterite/poly(lactic acid) composites. Acta Biomater 2009;5:57–62.
[20] Sugiura Y, Niitsu K, Saito Y, Endo T, Horie M. Inorganic process for wet silica-doping of calcium phosphate. RSC Adv 2021;11:12330–5.
[21] Sugiura Y, Ono F, Nohara M, Takechi A, Kutara K, Kanda T, et al. Inorganic silica hybrid octacalcium phosphate bone substitute: harmonics to acceleration in biological metabolism and its curing process. Materialia 2023;28:101771.
[22] Sugiura Y, Saito Y, Yamada E, Endo T, Horie M, Makita Y. Fabrication of silica-substituted carbonate apatite blocks through phase transformation process from silica-substituted octacalcium phosphate blocks. J Ceram Soc Jpn 2023;131:458–65.
[23] Sugiura Y, Saito Y, Yamada E, Endo T, Horie M. Fabrication of silica-substituted octacalcium phosphate blocks based on the setting reaction of the $CaCO_3$–H_3PO_4–Na_2SiO_3 cementing process. J Ceram Soc Jpn 2023;131:901–5.
[24] Sugiura Y, Saito Y, Yamada E, Endo T, Horie M. Fabrication of dicarboxylic-acid- and silica-substituted octacalcium phosphate blocks with stronger mechanical strength. Ceramics 2024;7:796–806.
[25] Sugiura Y, Makita Y. Intercalated molecule releasing process of thiomalate substituted octacalcium phosphate crystals during phase conversion. J Cryst Growth 2022;583:126545.
[26] LeGeros RZ, Trautz OR, Klein E, LeGeros JP. Two types of carbonate substitution in the apatite structure. Experient A 1969;25:5–7.
[27] Rey C, Collins B, Goehl T, Dickson IR, Glimcher MJ. The carbonate environment in bone mineral: a resolution-enhanced Fourier Transform Infrared Spectroscopy Study. Calcif Tissue Int 1989;45:157–64.
[28] Sugiura Y, Ishikawa K. Fabrication of carbonate apatite blocks from octacalcium phosphate blocks through different phase conversion mode depending on carbonate concentration. J Solid State Chem 2018;267:85–91.
[29] Wakae H, Takeuchi A, Udoh K, Matsuya S, Munar ML, LeGeros RZ, et al. Fabrication of macroporous carbonate apatite foam by hydrothermal conversion of a-tricalcium phosphate in carbonate solutions. J Biomed Mater Res A 2008;87A:957–63.
[30] Mladenovic Z, Johansson A, Willman B, Shahabi K, Björn E, Ransjö M. Soluble silica inhibits osteoclast formation and bone resorption in vitro. Acta Biomater 2014;10:406–18.
[31] Baig AA, Fox JL, Young RA, Wang Z, Hsu J, Higuchi WI, Chhettry A, et al. Relationships among carbonated apatite solubility, crystallite size, and microstrain parameters. Calcif Tissue Eng 1999;64:437–49.

[32] Vereecke G, Lemaitre J. Calculation of the solubility diagrams in the system $Ca(OH)_2$-H_3PO_4-KOH-HNO_3-CO_2-H_2O. J Cryst Growth 1990;104:820–32.
[33] Moorthi A, Parihar PR, Saravanan S, Vairamani M, Selvamurugan N. Effects of silica and calcium levels in nanobioglass ceramic particles on osteoblast proliferation. Mater Sci Eng C 2014;43:458–64.
[34] Ishikawa K. Bone substitute fabrication based on dissolution-precipitation reactions. Materials 2010;3:1138–55.
[35] Roelofs AJ, Stewart CA, Sun S, Błażewska KM, Kashemirov BA, McKenna CE, , et alCoxon FP. Influence of bone affinity on the skeletal distribution of fluorescently labeled bisphosphonates *in vivo*. J Bone Miner Res 2012;27:835–47.
[36] Flanagan AM, Chambers TJ. Nucleation and growth of mineral crystals in bone studied by small-angle X-ray scattering. Calcif Tissue Int 1991;49:407–13.
[37] Fournier PG, Stresing V, Ebetino FH, Clézardin P. How do bisphosphonates inhibit bone metastasis in vivo? Neoplasia 2010;12:571–8.
[38] Karashima S, Takeuchi A, Matsuya S, Udoh K, Koyano K, Ishikawa K. Fabrication of low-crystallinity hydroxyapatite foam based on the setting reaction of α-tricalcium phosphate foam. J Biomed Mater Res A 2009;88A:628–33.
[39] Zhao Y, Wong HM, Wang W, Li P, Xu Z, Chong EYW, et al. Cytocompatibility, osseointegration, and bioactivity of three-dimensional porous and nanostructured network on polyetheretherketone. Biomater 2013;34:9264–77.
[40] Nichols JE, Cortiella J, Lee J, Niles JA, Cuddihy M, Wang S, et al. *In vitro* analog of human bone marrow from 3D scaffolds with biomimetic inverted colloidal crystal geometry. Biomater 2009;30:1071–9.
[41] Kassebaum NJ, Bernabé E, Dahiya M, Bhandari B, Murray CJL, Marcenes W. Global burden of severe periodontitis in 1990-2010: a systematic review and meta-regression. J Dent Res 2014;93:1045–53.
[42] Haugen HJ, Lyngstadaas SP, Rossi F, Perale G. Bone grafts: which is the ideal biomaterial? J Clin Periodontol 2019;46:92–102.
[43] Suzuki S, Sugihara N, Kamijo H, Morita M, Kawato T, Tsuneishi M, et al. Reasons for tooth extractions in Japan: the second nationwide survey. Int Dent J 2022;72:366–72.
[44] Maeda K, Akagi J. Oral care may reduce pneumonia in the tube-fed elderly: a preliminary study. Dysphagia 2014;29:616–21.
[45] Sanchez P, Everett B, Salamonson Y, Redfern J, Ajwani S, Bhole S, et al. The oral health status, behaviours and knowledge of patients with cardiovascular disease in Sydney Australia: a cross-sectional survey. BMC Oral Health 2019;19:12.
[46] Taguchi Y, Yasui N, Takahashi S, Tominaga K, Kato H, Komasa S, et al. Hard tissue formation by human periodontal ligament fibroblast cells treated with an emdogain®-derived oligopeptide *in vitro*. J Hard Tissue Biol 2012;21:375–84.
[47] Takallu S, Kakian F, Bazargani A, Khorshidi H, Mirzaei E. Development of antibacterial collagen membranes with optimal silver nanoparticle content for periodontal regeneration. Sci Rep 2024;14:7262.
[48] Dong Z, Lin Y, Xu S, Chang L, Zhao X, Mei X, et al. NIR-triggered tea polyphenol-modified gold nanoparticles-loaded hydrogel treats periodontitis by inhibiting bacteria and inducing bone regeneration. Mater Des 2023;225:111487.
[49] Nasiri K, Masoumi SM, Amini S, Goudarzi M, Tafreshi SM, Bagheri A, et al. Recent advances in metal nanoparticles to treat periodontitis. J Nanobiotechnol 2023;21:283.